SLAC-PUB-10351
Mar 1 2004

An Ion Chamber System Used at High Instantaneous Rates ⋆

Clive Field *, Gholam Mazaheri

Stanford Linear Accelerator Center, Stanford University, Stanford, CA 94309, U.S.A.

G. Mark Jones

California Institute of Technology, Pasadena, California 91125, U.S.A.

Abstract

A radiation hard, compact, ion chamber detector system is described. The chambers are planar, with narrow gaps, and are filled with nitrogen gas. They operated at a signal rate equivalent to $\sim 2 \times 10^8$ minimum ionizing tracks per cm^2, delivered in pulses 250 ns long, while monitoring an intense scattered electron flux.

Key words: ion chamber, high intensity, radiation hard
PACS: 29.40.Cs, 07.77.Ka

Submitted to Nuclear Instruments and Methods in Physics Research A

⋆ Work supported by the U.S. Department of Energy, Contract DE-AC03-76SF00515

* Corresponding author. Tel.: + 1-650-926-2694; fax: +1-650-926-4178
Email address: sargon@slac.stanford.edu (Clive Field).

1 Introduction

High energy physics continues to explore ever more subtle effects, demanding ever higher statistical weight. This has led to the development of very intense beams, and techniques for high statistics monitoring of very high rates of interactions. In this paper we give an account of a detector capable of very high instantaneous rate, used as part of an experiment at the Stanford Linear Accelerator Center. The experiment, E-158 [1], measured the parity violating asymmetry $\sim 10^{-7}$ in the electron-electron (Møller, or ee) scattering rate as the electron beam polarization vector was reversed between forward and backward directions. The detector to be described, however, was used to test the null asymmetry expected in the higher rate electron-proton (ep) scatters.

The experiment made use of electron beams delivered at 45 and 48 GeV. At these energies, the beam intensities were as high as 5.5×10^{11} and 4.5×10^{11} per pulse respectively, with pulse lengths of approximately 250 ns. The beam, delivered at 120 Hz, passed through a 1.5 meter long liquid hydrogen target [2]. The exhaust beam, together with the bulk of ep and ee scatters, proceeded through a spectrometer built from a chicane of dipole magnets and quadrupoles. Within these were collimators to define the acceptance apertures, and to protect the detector for the ee scatters from direct gamma rays. The detector discussed here was intended to intercept a fraction of the electrons from the forward ep scatters in order to test for unexpected systematic biases. The opening angle was in the range of 1 mrad, and the intercepted rate of scattered electrons was about 3×10^8 per pulse, in order to allow the accumulation of 10^{17} scatters during the experiment to yield the necessary statistical weight.

The forward-going electrons from ep scatters were expected to be accessible far downstream in a ring of area ~ 100 cm^2 around the electron beam pipe, so the superficial intensity would be high. In fact the high radiation levels, and inaccessibility because of induced radioactivity, indicated that we should not rely on local amplifiers or other electronics. In addition, space available in the radiation shielded enclosure was limited.

The decision was made to use narrow-gap planar ion chambers for this application, since they can be radiation hard, capable of very high rates, and have stable sensitivity. The narrow gap was intended to reduce the time available for ion re-attachment, which otherwise could cause non linear response at high ion densities. The use of ion chambers as beam monitors under high intensity conditions has been reported [3]. In these cases, using helium gas, linearity was observed at up to 3×10^6 tracks per cm^2 in millisecond pulses, and 1.2×10^8 tracks per cm^2 in 10 ps pulses respectively. Ion chambers can be built to have small inefficient space at their edges, useful in the constricted

installation space of E-158.

The electron trajectories to be monitored proceeded in vacuum past the main ee detector. At 62 meters from the target, the radius of the vacuum pipe was decreased, using an aluminum flange 0.25 radiation lengths thick, allowing tracks to escape. Beyond the flange, the beam pipe outer radius was 7 cm, and the ep detector was placed around this. However, the acceptance was limited at about 9.5 cm radius because of the upstream acceptance-aperture collimator.

An additional complication was the synchrotron radiation from the beam line elements. With a range of critical energies close to 1 MeV, and intensities above 10^{11} per pulse above 0.1 MeV, this had the potential to dilute the signal of interest, if it were not filtered out. In fact, if the beam had a transverse component of polarization, this would modulate the rate of synchrotron radiation and lead to a false asymmetry[4]. In order to suppress this, a filter of 7.3 radiation lengths of aluminum was built. This took the form of pairs of half-rings machined to fit tightly around the beam pipe. For 1 MeV photons, this would reduce their intensity by a factor of 6×10^{-5}, adequate for our purposes. Of course, this also intensified the signal from the electrons by showering them.

To provide some information on systematic effects such as nonlinear performance, shower leakage and background asymmetries, a second ring of detectors was installed after a further 4.6 radiation lengths of aluminum. The layout is illustrated in Fig. 1.

2 Simulation studies

Since the detectors' window on the process of interest was so limited, it was thought wise, from the point of view of systematic effects, to understand the acceptance. A study with EGS4 [5] was carried out. In this, rays of electrons at various energies were directed into a representation of the vacuum flange, or at shallow angles into the vacuum side of the beam pipe. The assembly and detectors were modeled in the approximation of cylindrical geometry.

Since the aluminum filter was long, but the detector area limited relative to the transverse spread of the ionization, normal expectations for $\sim$ 45 GeV showers had to be reconsidered. Tracks aimed directly toward the middle of a detector spread some of their ionization beyond the acceptance of the first ring, and a considerably larger fraction missed the second ring. Conversely, tracks aimed at the front flange near the beam pipe aperture, or even at a shallow angle at the inside of the beam pipe, still contributed signal strength,

particularly to the rear ring. This relative enhancement of the rear signal at low radius may be seen in Fig. 2, where the simulated signal strength from 44 GeV tracks is plotted against the incident track radius (at the plane of the flange face). The simulation also showed that, for tracks at low radius, a significant fraction of the shower escaped into the beam vacuum, crossed over the beam pipe, and illuminated the rear ring of detectors on the opposite side.

The simulation used a parametrization of the transverse distribution of the incoming tracks. Their energy distribution was handled by weighting. Uncertainties, including the offset of the beam from the center of the pipe, were estimated by rerunning with parameters and geometry altered to their uncertainty limits. It will be referred to below, so we mention here that the ratio of signals simulated between front and rear rings was 2.94 ± 0.07. Background gamma rays from target and collimators were also studied in simulation, but shown not to contribute significantly.

3 Technical aspects of the detectors

A practical structure for the detectors involved assembling each ring from octants of individual ion chambers. The electrode plates were mounted perpendicular to the direction of the shower. In each chamber there were ten sequential sense gaps, each 0.8 mm deep, whose electrodes were of aluminum, 1.6 mm thick. This may be seen in Fig. 3.

The electrode package was spaced and held in alignment by three screws. The stainless steel screws were insulated with polyimide tape, and were threaded through oversize holes in the plates. The gap spacers were 6 mm square pieces of G-10, also mounted on the screws. After alignment, the screws were tightened until the package was rigid.

One outer corner of each plate had been cut short in fabrication. During assembly, the plates were stacked so that the short and long corners alternated. There were pre-drilled holes in the long corners, and these were aligned before rigidizing the package. A screw was self-tapped through each line of holes, thus connecting the package electrically into two alternating sets of plates. A pair of wires, in thin sleeves of glass-fiber, was used to connect these to BNC feedthroughs.

The stack of plates was fitted snugly into a tank. The wall between the plates and the beam pipe, and the neighboring chambers, was of 0.8 mm thick aluminum, formed to fit, and insulated internally with polyimide foil because of the proximity of the electrodes. This thin cover was screwed to relatively thick walls of aluminum, front, back and on the side away from the beam.

The chamber was sealed with epoxy[6]. The outer plate held two connectors for 1/8-inch copper gas tubes and the two radiation hard BNC electrical connectors[7], which had to be gas-sealed also.

It was decided to bring signals from both anode and cathode plates all the way from the shielded experimental area to an always-accessible electronics building. Connections at the chambers were made using radiation hard BNC connectors on RG58 cables 8 meters long. At this point, where radiation levels were lower, a transition was made to 80-meter long-haul foam-dielectric RG8 cables. In the electronics building, the cathode cables were each connected through a 1 MΩ resistor to a common bias voltage supply, typically operated at 100V. The signal pulse on each of these cables was coupled out capacitively (0.01 μF) to an RG174 cable. The anode cables were each grounded through 10 kΩ, and also passed on in RG174. Thus both electrodes and their connections had an unbroken grounded shield all the way to the remote electronics. The shield was isolated from all grounds except at the electronics units. This required insulating sections to be inserted in the copper gas lines.

Each pair of corresponding anode and cathode RG174 cables was presented to the differential input of an ADC channel. The ADCs, with six channels per VME card, had 16 bit resolution. They were developed for toroid signals for this experiment[9]. By using a differential input in our case, we intended to suppress common mode noise. No amplifiers were used.

The gas chosen was nitrogen at atmospheric pressure. In the difficult operating environment, this had the virtues of simplicity, ease of use and ruggedness. It had previously been used with good results[10] in an environment of intense picosecond gamma ray pulses. It is obviously radiation hard, and charge collection time was acceptable with the narrow gaps and strong field of 1260 V/cm used here. With a practical chamber design, nitrogen yielded sufficient signal strength to make amplifiers unnecessary.

The supply cylinder, regulator, safety valves and system flow control valves were outside the radiation area. A long 0.25 inch outer diameter copper line fed the gas to a filter mounted close to the chambers, and, through a manifold, to 16 flow adjustment valves before reaching the 16 chambers. The outflow from each chamber was brought to a low viscosity (10 centistokes) silicone oil bubbler mounted adjacent to the corresponding adjustment valve. The valve and bubbler were used at the beginning to balance the flow to each of the chambers so that the gas in the gaps was replaced about every 30 minutes. A miniature dynamic microphone[8] was pressed against the polystyrene test-tube containing each bubbler's fluid, and these were monitored, via twisted pair cables, in the electronics room, allowing all the flow rates to be logged remotely. It was found that small strips of metal between the tube and the microphone could be tuned to shift the sound spectrum and enhance the

detection of bubble noise in the range 1 to 3 kHz.

4 Operational experience

During initial investigations, signals were observed from the chambers with bias voltages from 0.5 V upwards. The electron drift time decreased markedly, of course, as the voltage was increased. The decay times (between 90% and 10% of peak amplitude) were 1000 ns at 0.5V, 300 ns at 2V, 140 ns at 10V and 125 ns at 100V. The charge collection efficiency had reached a plateau with the bias as low as 20 volts. However, the operating voltage was chosen to be 100V, or 1260V per cm of gap, to help maintain linearity at high ionization densities.

Samples of the pulse shapes are given in Fig. 4. Traces for both positive going (capacitively coupled) and negative going (direct coupled) pulses from a chamber are shown. The rounded top of the pulse is largely determined by the profile of the ∼250 ns wide beam pulse. The rising and trailing edges are characteristic of the ion chamber and cable system. For comparison, Fig. 5 shows pulses obtained during tune-up when the beam pulse length was a few picoseconds long.

Each chamber was sensitive not only to beam intensity, but also energy fluctuations and beam steering angle, approximately as $E^{-2}\,\theta^{-4}$. The beam intensity during data taking was well controlled, fluctuating by typically 0.9% rms. It was found that the beam, and the center of the distribution of the scattered tracks, was pointed off-center relative to the ring of detectors. This contributed a relatively stable difference of 30% between the largest signals and the smallest, on opposite sides of the ring. Pulse-to-pulse fluctuations in this steering caused signal fluctuations which were reduced to 0.8% by summing signals around the ring of detectors.

Together with the limited precision with which beam angle and position could be measured close to the ion chambers, these small but comparable influences on signal strength made it difficult to obtain a direct estimate of the detector's linearity of response from the small beam intensity fluctuations in the production data set. On the other hand, perhaps in 50 pulses in a million, a random fault in the accelerator would cause the beam intensity to be low by up to two orders of magnitude. We now discuss how these pulses have been used as an indication of the chambers' response. For these individual cases, energy and steering parameters may have been off-center within the beam acceptance limits. We estimate that this could broaden the signal vs. beam-intensity correlation by ∼1%, based on the excursions seen under normal beam conditions.

A data set with 1.1×10^6 pulses, approximately three hours of beam delivery, was examined. In this set the mean beam pulse intensity was 5.2×10^{11}. We selected the few individual pulses below 4.16×10^{11}, i.e. below 80% of the mean intensity. For these pulses, the front ring signals were plotted against a toroid signal, Fig. 6. It should be noted that the correlation between different toroids was linear, with fluctuations below the 10^{-3} level. In order to fit the ion chamber vs. toroid data, the signals were weighted to allow for energy- or steering-induced fluctuations whose size is proportional to intensity, as well as a constant term, consistent with what was observed. Straight line fits were applied to the points with toroid signals from 0.01×10^{11} up to various limits from 2.6×10^{11} to 4.16×10^{11}. The details of weighting did not affect the straight line fit significantly. The fit lines were extrapolated into the toroid range of the normal beam condition to test for consistency.

The good-beam data exhibited tendencies for $\sim$1% fluctuations and drifts, with correlation trends depending on energy and steering that varied from time to time. Dealing with these represented the challenge in obtaining physics asymmetry results[1], and will not be reviewed in this discussion. The task here was to counter the high statistical power of these data to skew any fit, because of short range internal correlations that are irrelevant for testing linearity. For this purpose, the 1.1×10^6 data points above the 80% intensity division were simply averaged, giving the mean intensity of 5.2×10^{11}. This point is also plotted in Fig. 6. As an indication of the stability of the beam, the RMS ranges — not the standard errors — are shown by the bars.

The high intensity point is consistent with the extrapolated straight line fits. For example, extrapolating the 0.01×10^{11} to 2.6×10^{11} fit, it was found that all points above this fall within $\pm$1.55% of the line, and the high statistics point within 0.21% of it. When a quadratic or a cubic term was added to the fit expression, the extra term was significant in either case at the 3 standard deviation level, but the unfitted points above 2.6×10^{11} mostly lay above the fit line. In particular the unfitted high statistics point was above the regression line by 1.7% for a quadratic term and 4.2% for a cubic.

When all points, including the high statistics 5.2×10^{11} point, are included, the straight line shown in Fig. 6 is obtained. All points with beam intensity above half of the peak are within 1.34% of the line, which essentially goes through the 5.2×10^{11} point. It is unnecessary to add a quadratic or cubic term to the fit. The fitted coefficient of a quadratic term is only 9% of its uncertainty, and that of a cubic is 54% of its uncertainty. The fractions of the signal coming from the higher order terms are 1.7×10^{-4} and -1.3×10^{-3} respectively, at intensity 5.2×10^{11}. We conclude that there is no indication of a chamber saturation effect as large as 1% up to this beam intensity.

As a check for other unexpected systematic effects, we have also compared sig-

nal amplitudes in the front and rear rings of chambers. During an interval at low repetition rate, while physics data were not being collected, signals were recorded by digital oscilloscope. The average ratio between front and back signals was measured by oscilloscope to be 2.96 ± 0.05 at a beam intensity of 5.5×10^{11} per pulse, the maximum used for data taking. In this way, possible effects caused by the ADC channel sensitivities were removed. The ratio was also calculated run by run for some normal data using the electronics system. From this the ratio was measured to vary by ± 0.03 about 2.86. However, under these 120 Hz conditions the showering in the aluminum caused a marked increase in temperature. At the front chambers, the temperature reached as high as 54°C under some conditions. The rear chambers, in the tail of the shower, were typically 12° lower. Correcting for the consequent density difference in the chamber gas, the front to back ratio during data taking would have been 2.92, agreeing with the oscilloscope value.

As mentioned above, the system was simulated using the EGS4 shower code assuming cylindrical symmetry, and the ratio of signals, front : rear, was estimated at 2.94 ± 0.07. This agreement with observation is evidence that the scattering from the target, acceptance and performance of the system are adequately understood. It may be taken as independent confirmation of linearity, at least at the 3% level. In this case, the test range for linearity is $\times 3$ in signal strength, up to a beam intensity of 5.5×10^{11}. The mean charge developed in the gaps under these conditions was 22 nC per chamber per pulse, or approximately 1.8 nC per cm^2 per pulse. This corresponds to 2.3×10^8 minimum ionizing tracks per cm^2 per 250 ns pulse [11].

For its contribution to the physics results from the experiment, the detector analysis, outlined in [1], made the assumption that each octant was sensitive approximately linearly to small shifts in the various measured beam steering parameters, energy and intensity. An iterative fitting procedure was carried out to determine an optimum combination of dependencies. The data was normalized to toroid readings so that the two sets of pulses with opposite beam polarizations could be compared. This was done for each "run" of $\sim 400,000$ pulses. Using this procedure to estimate the remaining apparent intrinsic pulse-to-pulse fluctuation level of the system, including the ADCs, gave values as low as 105 ppm. Approximately 30% of the data has so far been processed for publication, and the beam-polarization-dependent overall asymmetry ((right handed - left handed) / sum) has been measured as $(-16 \pm 15) \times 10^{-9}$ [1], consistent with theoretical expectations for the ep scatters.

5 Conclusions

At the termination of the experiment, the detectors at the most intense part of the shower had accumulated a radiation dose estimated to be 7×10^9 Rads from the ep scatters. As measured by survey personnel, the radioactivity level induced in the detector at the end of the final run was 2 R/hr on contact. Self induced ion current from this activity was not an issue, given the short SLAC duty factor. Although the detectors were, of necessity, radiation hard, they also were inexpensive and expendable. Despite this, they remained gas tight and no electrical changes were encountered. The system provided a stable, high sensitivity to the high rate of electrons from this experiment, and has recorded an effective statistical weight of about 4×10^{17} incident tracks.

6 Acknowledgments

We are grateful to SLAC accelerator department for their skillful and dedicated delivery of the intense and tightly controlled beam that made this detector both necessary and useful. We also thank the others of the E-158 collaboration for their support and their work in collecting the data and in analysis. In particular we thank Drs. Lewis Keller and David Relyea whose distributions of simulated trajectories we parametrized for the detector simulation. One of us (M.J.) wishes to thank Prof E. Hughes for support and encouragement. We are grateful to the Department of Energy and the National Science Foundation for their support of this experiment.

References

[1] P. Anthony *et al.*, ArXiv hep-ex0312035, submitted to Phys. Rev. Letters.

[2] J. Gao *et al.*, Nucl. Instr. and Meth. A 498 (2003) 90.

[3] R. Blair *et al.*, Nucl. Instr. and Meth. 226 (1984) 281; J. McDonald *et al.*, Nucl. Instr. and Meth. A 496 (2003) 293.

[4] A.E. Bondar and E.L. Saldin, Nucl. Instr. and Meth. 195 (1982) 577.

[5] W.R. Nelson *et al.*, SLAC-265, Dec. 1985 (unpublished).

[6] Hysol Epoxy-Patch 1C: Dexter Corporation, Seabrook, NH, U.S.A.

[7] Tru Connector Corp, Peabody, Mass. U.S.A. UG-657/U, Rexolite dielectric.

[8] Knowles Electronics, Franklin Park, Il, U.S.A.; Part no. BJ-1590.

[9] Integrating ADC VME Module for E-158, G. Haller, K. Kumar and P. Anthony, SLAC (unpublished); Module 922-158-01 based on Maxim MAX1200 ADC chip (contact G. Haller).

[10] C. Field, G. Mazaheri and J.S.T. Ng, Nucl. Instr. and Meth. A 489 (2002) 68.

[11] A.V. Zarubin, Nucl. Instr. and Meth. A283 (1989) 409, table 2.

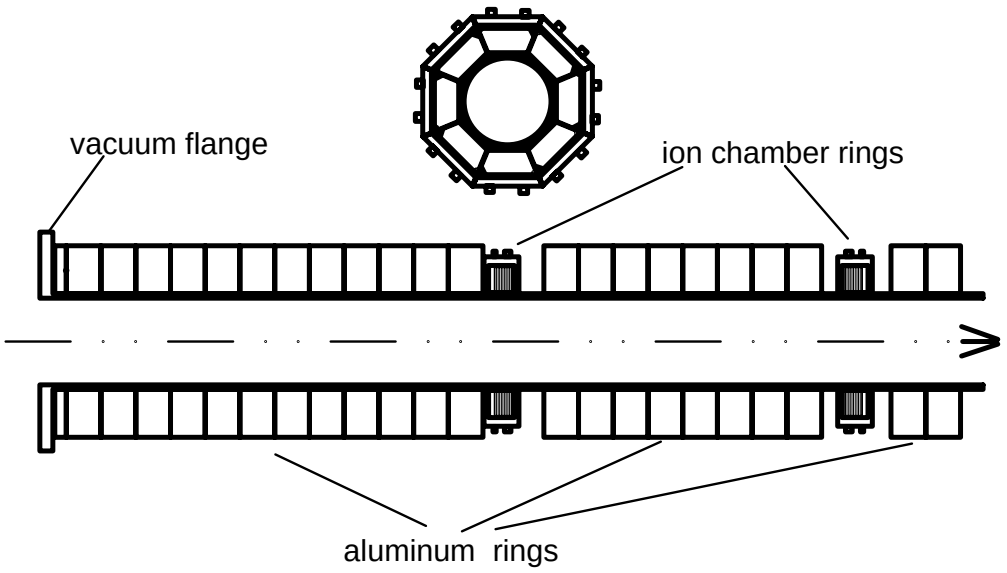

Fig. 1. Schematic longitudinal section through the detector system, and (above) a transverse section through a ring of eight ion chambers. The length of the beam pipe shown is 140 cm. The direction of the electron beam is indicated by the arrowhead on the right.

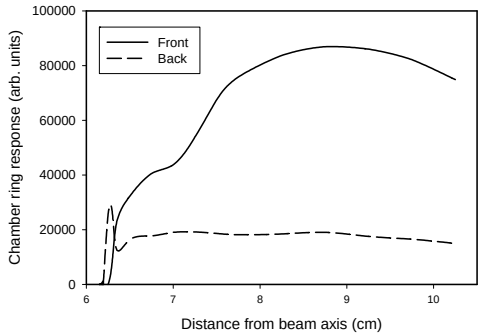

Fig. 2. Simulation of the expected signals in front and back rings as a function of the radius of incidence of initiating electrons of 44 GeV. The sharp peak at low radius in the back chamber curve is caused by tracks striking the relatively thin beam pipe at glancing angles. It can be seen that the front : back ratio varies considerably.

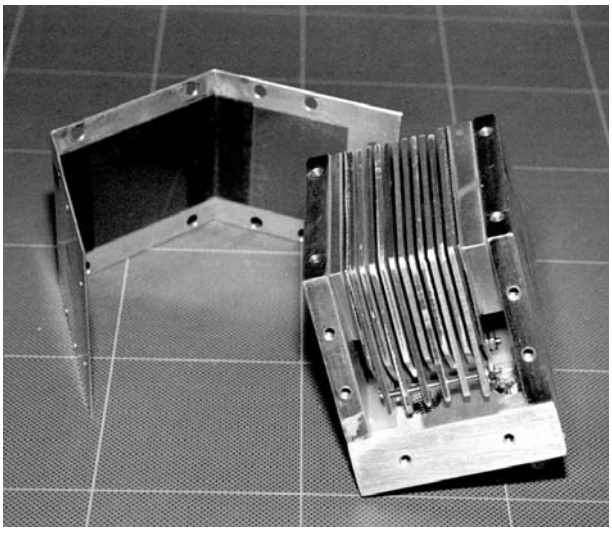

Fig. 3. Photograph of an ion chamber with the thin cover removed. The stack of electrode plates is clearly visible. The screw connecting the anode plates electrically can also be seen.

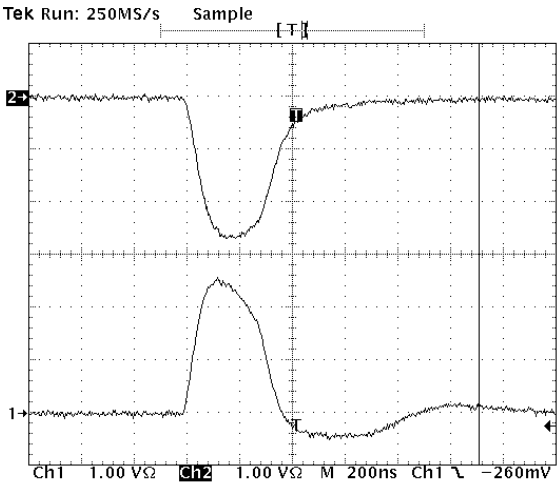

Fig. 4. Oscilloscope trace from a chamber for a 5.5×10^{11}, 250 ns long, beam pulse. The anode and capacitively-coupled cathode signals are shown.

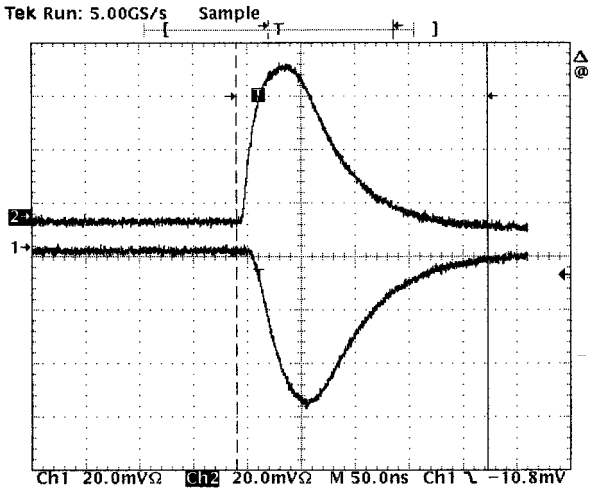

Fig. 5. Oscilloscope trace from a chamber with a beam pulse < 10 ps long, 5×10^9 per pulse.

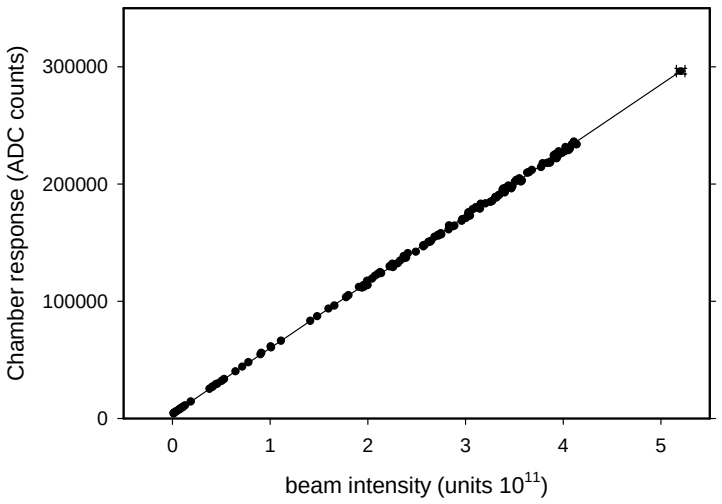

Fig. 6. Pulse height vs. beam intensity measured by a toroid. Individual pulses are shown for toroid readings below 4.16×10^{11}. Above this, 1.1×10^6 pulses are averaged and shown with the rms range, rather than the standard error (illustrating the stability of the beam under normal conditions). A straight line fit to all points is also shown.